UC Riverside
UC Riverside Previously Published Works

Title

Building blocks for bioinspired electrets: molecular-level approach to materials for energy and electronics

Permalink

Journal

ISSN

Authors

Larsen, Jillian M
Espinoza, Eli M
Hartman, Joshua D
et al.

Publication Date

DOI

Peer reviewed

DE GRUYTER

Pure Appl. Chem. 2015; 87(8): 779–792

Conference paper

Jillian M. Larsen, Eli M. Espinoza, Joshua D. Hartman, Chung-Kuang Lin, Michelle Wurch, Payal Maheshwari, Raman K. Kaushal, Michael J. Marsella*, Gregory J. O. Beran* and Valentine I. Vullev*

Building blocks for bioinspired electrets: molecular-level approach to materials for energy and electronics

Abstract: In biology, an immense diversity of protein structural and functional motifs originates from only 20 common proteinogenic native amino acids arranged in various sequences. Is it possible to attain the same diversity in electronic materials based on organic macromolecules composed of non-native residues with different characteristics? This publication describes the design, preparation and characterization of non-native aromatic β-amino acid residues, i.e. derivatives of anthranilic acid, for polyamides that can efficiently mediate hole transfer. Chemical derivatization with three types of substituents at two positions of the aromatic ring allows for adjusting the energy levels of the frontier orbitals of the anthranilamide residues over a range of about one electronvolt. Most importantly, the anthranilamide residues possess permanent electric dipoles, adding to the electronic properties of the bioinspired conjugates they compose, making them molecular electrets.

Keywords: amino acids; biomimetic synthesis; dipole; electrets; electrochemistry; electronic structures; microwave synthesis; NICE-2014; photophysics; reduction potentials.

Introduction

Charge transfer (CT) drives almost any phenomenon known to us from a molecular to macroscopic scale. At a cellular level, CT is responsible for a range of chemical and biochemical transformations, and is essential for life on Earth to exist [1–5]. In addition to its vital role in living systems, CT resides at the heart of energy conversion, transduction and storage [6–13], and provides signal transduction for devices integral to our modern lifestyles [14, 15]. For more than a century, the key importance of CT has sustained the ever-growing scientific interest in it.

*Corresponding authors: Valentine I. Vullev, Department of Bioengineering, University of California, Riverside, CA, 92507, USA; Department of Chemistry, University of California, Riverside, CA, 92507, USA; Department of Biochemistry, University of California, Riverside, CA, 92507, USA; and Materials Science and Engineering Program, University of California, Riverside, CA, 92507, USA, e-mail: vullev@ucr.edu; and **Gregory J. O. Beran and Michael J. Marsella,** Department of Chemistry, University of California, Riverside, CA, 92507, USA, e-mail: gregory.beran@ucr.edu (G. J. O. Beran), michael.marsella@ucr.edu (M. J. Marsella)
Jillian M. Larsen, Chung-Kuang Lin, Michelle Wurch, Payal Maheshwari and Raman K. Kaushal: Department of Bioengineering, University of California, Riverside, CA, 92507, USA
Eli M. Espinoza and Joshua D. Hartman: Department of Chemistry, University of California, Riverside, CA, 92507, USA

Among the four fundamental forces in the universe, electromagnetic interactions are the second strongest, weaker only than the nuclear strong force [16]. Unlike nuclear forces, however, electromagnetism prompts long-range interactions making it deterministic for condensed matter [17]. Even minute displacement of charges can result in macroscopically observable phenomena [18–28]. Similarly, with the development of metamaterials, controlling nanometer-scale CT allows for an emergence of unprecedented properties.

The value of the capability to control CT at molecular and nanometer scales cannot be overstated. The utility of local electric fields, generated from molecular and macromolecular dipoles, for ion transport and electron transfer is paramount for living systems [29–31]. Hence, molecular electrets present an important paradigm for guiding CT. (Dipole-polarization electrets are the electrostatic analogues of magnets, i.e. they possess co-directionally ordered electric dipole moments.)

Protein helices represent one of the best examples for molecular electrets, and their electronic properties are essential for various processes in biology [29, 30]. Biomimetic systems, based on polypeptide helices comprising native α-amino acids, rectify the directionality of CT [32–36]. These protein structures, however, possess drawbacks that are inherent to electret materials. Electrets are dielectrics and they may not contain free charge carriers. Free-moving charges in the electret or in the surrounding media would screen the dipole-generated fields eliminating the dipole effect. Hence, electron tunneling is representative of the prevalent mechanism of CT mediated by biological and biomimetic polypeptide structures [37–43]. Tunneling, however, limits the distance of efficient CT to about 2 nm [37, 38]. Sites where charges can temporarily reside (such as redox active cofactors, nucleotides, or amino-acid side chains) can greatly extend the CT distance beyond the 2-nm tunneling limit [5, 44]. Good electronic coupling between a sequence of redox moieties ensures pathways for efficient multiple electron tunneling short steps allowing long-range CT to occur, i.e. long-range electron or hole hopping [5, 44].

To address some of the challenges with polypeptide biological and biomimetic structures, we have undertaken a bioinspired approach to designing molecular electrets in the search of properties that are beyond what natural systems can offer [45–48]. Composed of anthranilamide (**Aa**) residues, the bioinspired electrets possess ordered amide and hydrogen bonds that, similar to the ordered peptide bonds in protein helices, generate an axial electric dipole (Fig. 1). In addition to determining that these oligomers of aromatic *ortho*-amino acids are indeed molecular electrets [46], we also demonstrated that the **Aa** dipole rectifies charge transfer [45]. Furthermore, derivatizing an anthranilamide with a secondary amine as R_2 at the 5th position (Fig. 1), yields a residue that not only is a good electron donor, but also can host a positive charge for seconds as evident from the reversible electrochemical oxidation [45]. The ability to accommodate positive charges is a promising feature for mediating CT via hole (h^+) hopping.

Chemical derivatization provides a means to widely diversify the electronic properties of the **Aa** residues. With all *trans* amide bonds, the **Aa** oligomers assume an extended conformation, which also is key for their intrinsic dipole. To maintain this extended conformation, it is essential to prevent steric hindrance between residues proximal within an oligomer sequence. Therefore, only the distal sites, i.e. the 4th and 5th position in the aromatic rings of the residues (corresponding to R_1 and R_2, respectively, on Fig. 1), are available for chemical derivatization.
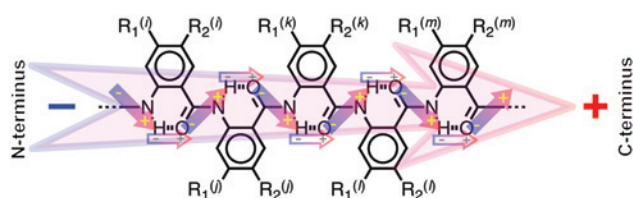
Fig. 1: Bioinspired molecular electret composed of anthranilamide residues (---**Aa**(i) − **Aa**(j) − **Aa**(k) − **Aa**(l) − **Aa**(m)---) and the origin of its electric dipole from the ordered orientation of the amide linkers and the polarization of the hydrogen bonds.

Each of the 20 native amino acids differs from the rest by only a single side chain. The side chains of these α-L-amino acid residues govern the conformational folds, and overall the protein structural and functional features. Conversely, the non-native anthranilic residues have two side chains (R$_1$ and R$_2$, Fig. 1) that can be used for adjusting their electronic properties. To explore the potential of these bioinspired molecular electrets as CT-controlling materials it is paramount to design a set of non-native **Aa** residues with diverse electronic characteristics.

Aromatic *poly-* and *oligo-*amides, such as Huc's foldamers [49–51], provide incomparable venues for exploring biological types of structural motifs, the diversity of which expands beyond what the natural systems can offer [52–56]. Indeed, the rich π-conjugation of such foldamers governs their immensely promising CT characteristics [57]. Our focus, conversely, is on extended aromatic structures, such as **Aa** oligomers (Fig. 1) [46, 48, 58], which are not truly foldamers. While the common theme as electrets with extended conformations and large intrinsic dipoles is conserved in the **Aa** structures, alterations of the side chains (R$_1$ and R$_2$, Fig. 1) provides venues for achieving diversity in the electronic properties of such aromatic *poly* and *oligo*-amides.

Herein, we demonstrate the preparation and characterization of eight non-native **Aa** residues with their N- and C-termini capped as alkyl amides (Fig. 2). In addition to the basic anthranilamide residue (Ant) where R$_1$ = R$_2$ = H, we investigate **Aa** derivatives with three types of electron-donating substituents for R$_1$ and R$_2$: alkyl (i.e. methyl), alkyoxyls (i.e. methoxy and hexyloxy groups) and amines (i.e. piperidinyl and hexylmethylamine). Electrochemical and spectroscopy studies allowed for estimating the energy levels of the frontier orbitals of these **Aa** residues. Density functional theory (DFT) calculations yielded information about the intrinsic electric dipoles of the **Aa** derivatives and provided visualization of their highest occupied and lowest unoccupied molecular orbitals (HOMO and LUMO, respectively).

In agreement with the contribution from the amide and hydrogen bonds [48], the magnitudes of the dipole moments of the **Aa** residues exceed 4 D. The chemical derivatization with the three listed electron-donating groups at the two positions of the **Aa** aromatic ring (i.e. the 4th and 5th) allow for adjusting the reduction potentials of the **Aa** oxidation over the range of about 1 V. This range is quite significant: adjusting the HOMO energy levels over 1 eV provides an incomparable means for modulating the hole-transfer pathways along sequences composed of such **Aa** residues.

In addition, the results demonstrate that the electronic properties of **Aa** depend on both the type of substituted groups used and the exact position of these groups. That is, an electron-donating group (EDG) as a substituent at the 4th and 5th positions can yield three distinct **Aa** residues with different electronic properties. A residue with R$_1$ = EDG and R$_2$ = H has different properties from a residue with R$_1$ = H and R$_2$ = EDG that also differs from a residue with R$_1$ = EDG and R$_2$ = EDG. This feature demonstrates diversity in electronic characteristics that can be achieved via permutations within a single **Aa** residue, something that native amino acids with single side chains cannot offer. It illustrates some of the advantages of bioinspired over biomimetic approaches [47].
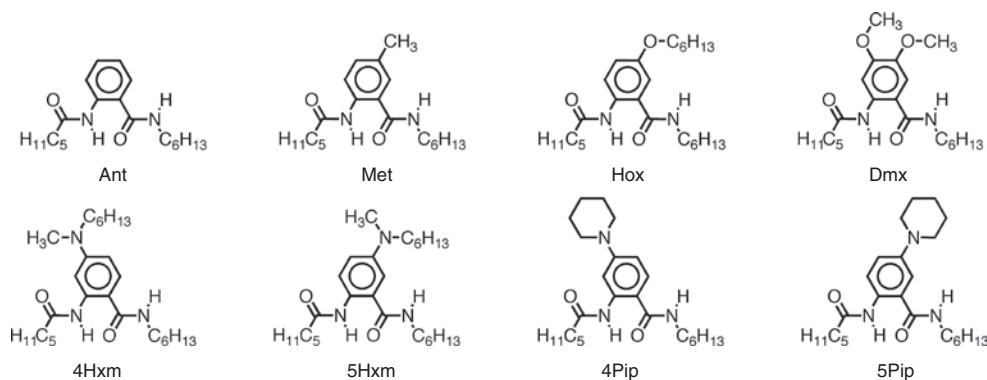

Fig. 2: Anthranilamide residues.

Results

Preparation of the anthranilamide residues

As polypeptide conjugates of aromatic non-native β-amino acids, we build the **Aa** oligomers from their C- to their N-termini [46]. Each **Aa** residue is added to the sequence as a 2-nitrobenzoic acid derivative [45, 46]. A selective reduction of the nitro group to amine prepares the thus added N-terminal residue for the next amide-coupling step [46]. The use of "traditional" synthetic protocols, where each residue is introduced as an N_β-Fmoc or N_β-tBoc anthranilic acid derivative, renders negligible to no yields. The electron-withdrawing nitro group at *ortho* position ensures the electrophilicity of the carbonyl carbon of the activated carboxylate that is needed for coupling it with the N-terminal amine. The N-terminal anthranilic amines are weak nucleophiles due to the neighboring electron-withdrawing carbonyls.

To attain a diversity of **Aa** residues, we focus on the preparation of a variety of 4- and 5- derivatives of the 2-nitrobenzoic acid as precursors for non-native **Aa** residues. Three types of substituents at R_1 and R_2 positions (Fig. 1) allow for producing electron-rich **Aa** residues with a wide distribution of the energy levels of their frontier orbitals: (1) strong electron-donating groups, dialkylamines; (2) moderately strong electron-donating groups, alkoxyls; and (3) a weak electron-donating group, methyl. Starting with fluoro-derivatives, nucleophilic aromatic substitution allow for introducing amines as substituents at the 4th and 5th positions of the 2-nitrobenzoic acid. In the 5-fluoro-2-nitrobenzoic acid, the C–F bond at the *para* position in relevance to the nitro group is quite polarized, making that carbon susceptible to the attack from an amine nucleophile. Using a cyclic secondary amine, i.e. piperidine, requires relatively short reaction times under conventional heating to produce in quantitative yields the nitrobenzoic precursor for the 5Pip residue (Scheme 1a) [45]. In the 4-fluoro-2-nitrobenzoic acid, the C–F bond is not as polarized due to the *meta* (rather than *para*) position of the nitro group. For the precursor for the 4Pip residue, therefore, the same nucleophilic aromatic substitution with the 4-fluoro-2-nitrobenzoic acid requires longer reaction times for attaining similar yields (Scheme 1b).

A synthetic challenge arises when the nucleophiles are non-cyclic secondary amines. Entropic restrictions decrease the nucleophilic reactivity of dialkylamines as the length of their chains increases [59]. Under conventional heating, the substitution of fluorine in 4-fluoro-2-nitrobenzoic acid with hexylmethylamine leads to negligible yields even when the reaction proceeds for unreasonably long periods of time (Scheme 1c).

Utilizing microwave radiation as a heat source allows for addressing this challenge. Although still debated, microwave heating may enhance reaction rates via the entropy components of their activation energies [60, 61], making it appropriate for overcoming the limitations imposed by amine nucleophiles with long alkyl chains. Employing microwave heating, indeed, allows us to develop procedures that lead to completion of the syntheses of the hexylmethylamino precursors for 4Hxm and 5Hxm (Fig. 2) within reasonable time durations (Scheme 1c,d).

The starting material for the Hox precursor is 5-hydroxy-2-nitrobenzoic acid, the carboxylate and the phenolate of which are indiscriminately strong nucleophiles readily producing the dialkyl derivatives. An extra hydrolysis step leads to the Hox nitrobenzoic precursor (Scheme 1e). Coupling of the 2-nitrobenzoic acids with 1-hexylamine, followed by selective reduction of the nitro group to amine and another amide coupling produces the eight **Aa** residues [45].

Reduction potentials

Electrochemical studies allow for quantifying the propensity of the **Aa** residues to serve as electron donors and to potentially mediate hole transfer. The reduction potentials of the oxidation of the **Aa** residues (i.e. $E^{(0)}_{\mathrm{Aa}^{\bullet+}/\mathrm{Aa}}$: $\mathbf{Aa}^{\bullet+} + e^- \to \mathbf{Aa}$) provide a means for quantifying their electron-donating capabilities [62], and for estimating the energy levels of their HOMOs [63].

To elucidate the media effects on the electronic properties, we focus on the dependence of the **Aa** electrochemical potentials on the solvent polarity [64–68]. Our selection includes five aprotic solvents with different
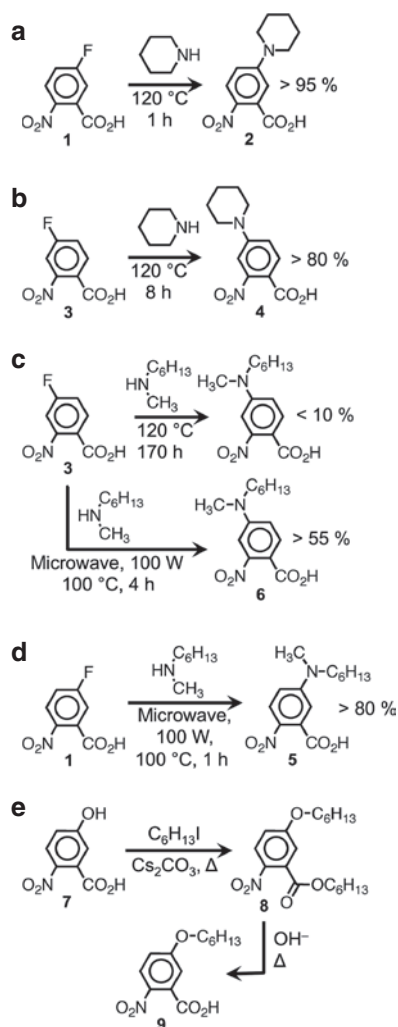
Scheme 1: Syntheses of the 2-nitrobenzoic acid precursors for (a) 5Pip, (b) 4Pip, (c) 5Hxm, (d) 4Hxm, and (e) Hox.

polarity that have electrochemical windows extending over the expected potentials needed for the oxidation of the **Aa** residues: chloroform (CHCl$_3$), dichloromethane (DCM), benzonitrile (PhCN), acetonitrile (MeCN), and propylene carbonate (PC).

As a representation of the standard electrode potentials, $E^{(0)}$, the half-wave potentials, $E^{(1/2)}$, are readily obtained from cyclic voltammetry (CV). For reversible electrochemical oxidation, $E^{(1/2)}$ represents the average between the peak potentials of the anodic and the cathodic waves. If the lifetimes of the radical cations, **Aa**$^{\bullet+}$, generated on the surface of the working electrode do not extend over milliseconds and seconds (the time scales of CV), the cathodic wave becomes undetectable. For such electrochemically irreversible oxidation, the potential at the inflection point of the rise of the anodic wave provides an estimate for $E^{(1/2)}$ (see Supplementary Material). 5Hxm, 5Pip, and Dmx manifest electrochemically reversible oxidation indicating that these residues produce radical cations with pronounced stability.

While electrochemical measurements require media with high electrolyte concentrations, it is the information for $E^{(0)}$ in neat solvents that is directly relevant to spectroscopy and computational data [65]. From the dependence of the measured $E^{(1/2)}_{\text{Aa}^{\bullet+}/\text{Aa}}$ on the electrolyte concentration, C_{el}, therefore, we extrapolate the values of the reduction potentials of the residues for zero electrolyte concentration, i.e. the **Aa** potentials for neat solvents, $E^{(C_{el}=0)}_{\text{Aa}^{\bullet+}/\text{Aa}}$ (Fig. 3a) [65].

Based on the Born solvation energy [69], a linear correlation between $E^{(C_{el}=0)}_{\text{Aa}^{\bullet+}/\text{Aa}}$ and the inverse dielectric constant of the neat solvents, ε^{-1}, reveals the effects of the media polarity on the electrochemical properties
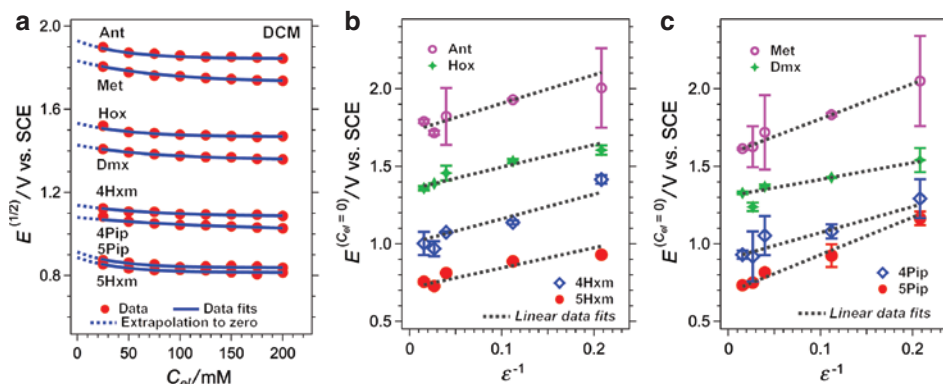
Fig. 3: Solvent dependence of the electrochemical potentials of the anthranilamide residues. (a) Dependence of the half-wave potentials of the **Aa** residues on the electrolyte concentration, C_{el} (for DCM in the presence of $(C_4H_9)_4NPF_6$ as electrolyte). Extrapolation to zero electrolyte concentration from exponential data fits provides the estimates for the reduction potentials of the residues in neat solvents. (b, c) Dependence of the extrapolated potentials for neat solvents on the media dielectric characteristics obtained from measurements for five different solvents: propylene carbonate, PC ($\varepsilon^{-1} = 0.016$); acetonitrile, MeCN ($\varepsilon^{-1} = 0.027$); benzonitrile, PhCN ($\varepsilon^{-1} = 0.040$); dichloromethane, DCM ($\varepsilon^{-1} = 0.11$); and chloroform ($\varepsilon^{-1} = 0.21$).

of each **Aa** residue (Fig. 3b,c). As expected, an increase in the solvent polarity (i.e. a decrease in ε^{-1}) shifts the potentials to less positive values, elevating the energy levels of the HOMOs, and improving the capabilities of the residues as electron donors (Fig. 3b,c). The stabilization of the radical cations, **Aa•⁺**, by polar media accounts for this negative shifts of the measured potentials.

For each solvent, an increase in the electron-donating strength of the substituents, from methyl to amines, causes negative shifts in the reduction potentials. The potential of the best electron donor, 5Hxm, is about 1 V more negative than that of Ant (Fig. 3b, Table 1). This finding is consistent with our theoretical predictions that placing dialkylamine at the 5th position of anthranilamides elevates the energy levels of their HOMOs with about 1 eV [48].

While the amine-derivatized **Aa** residues are the best electron donors, moving the amine substituents from the 4th to the 5th position causes another negative shift (of about 0.2–0.4 V) in the potentials (Fig. 3b,c). The alkylamines in 5Pip and 5Hxm are *para*-oriented to the electron-donating N-terminal amide and *meta*-oriented to the electron-withdrawing C-terminal amide. This *para*-orientation between the two

Table 1: Electronic characteristics of the anthranilamide residues.[a]

	R$_1$	R$_2$	μ^b/D			E^c/V vs. SCE		$\mathscr{E}_{00}{}^d$/eV	
			Vacuum	DCM	MeCN	DCM	MeCN	DCM	MeCN
Ant	H	H	4.71	6.38	6.68	1.93	1.72	3.7	3.7
Met	H	CH$_3$	4.96	6.79	7.12	1.83	1.63	3.6	3.6
Hox	H	OC$_6$H$_{13}$	6.42	8.56	8.96	1.53	1.39	3.4	3.5
Dmx	OCH$_3$	OCH$_3$	4.53	6.37	6.72	1.43	1.24	3.6	3.6
4Pip	N(CH$_2$)$_5$	H	4.46	6.26	6.62	1.08	0.919	3.6	3.7
5Pip	H	N(CH$_2$)$_5$	5.52	7.61	8.00	0.923	0.750	3.0	3.0
4Hxm	N(CH$_3$)C$_6$H$_{13}$	H	4.42	6.31	6.69	1.14	0.968	3.7	3.7
5Hxm	H	N(CH$_3$)C$_6$H$_{13}$	6.59	8.85	9.24	0.887	0.727	3.0	3.0

[a]From experimental and theoretical studies of the eight residues where R$_1$ and R$_2$ correspond to the 4th and 5th positions, respectively, in the aromatic rings (Figs. 1 and 2). [b]Dipole moments are obtained from DFT calculations for gas phase (vacuum) and for structures where the solvents, DCM and MeCN, are implemented as dielectric continua. The orientation of the molecular dipoles is from the N to the C-termini of the anthranilamide residues. [c]Reduction potentials for the residue oxidation, **Aa•⁺** + e^- → **Aa**, i.e. for neat solvents obtained from extrapolation of half-wave potentials to zero electrolyte concentration (Fig. 3a). [d]The zero-to-zero energy from the crossing point of the normalized absorption and fluorescence spectra (Fig. 4).

electron-donating groups in 5Pip and 5Hxm can account for the more negative values of their potentials in comparison with 4Pip and 4Hxm.

This "reinforcement" from two electron-donating groups *para*-positioned to each other can account for stabilizing the radical cations, **Aa•+**, and the reversible electrochemical oxidation of 5Pip and 5Hxm. This argument should hold also for the other electron-donating groups at the 5th position. While Dmx manifests reversible oxidation, however, the cyclic voltammograms of Hox and Met exhibit irreversible behavior. Despite the stabilization that 5-methyl and 5-hexyloxy groups might provide to the racial cations of Met and Hox, respectively, their reduction potentials appear positive enough to irreversibly cleave the amide bonds attached to the aromatic rings [70].

Photophysical properties

While electrochemical analysis provides information about the capabilities of the **Aa** residues to serve as electron donors and hole transducers, optical spectroscopy reveals complementary features about the energetics of the **Aa** frontier orbitals. In particular, UV/visible absorption and fluorescence spectroscopy provide a means for estimating the zero-to-zero energies, $\mathscr{E}_{00}$. $\mathscr{E}_{00}$ represents optical HOMO-LUMO gaps, which in molecular photophysics can be viewed as the optical band gaps of these **Aa** building blocks for organic materials.

The eight **Aa** residues absorb in the UV spectral region and fluoresce with substantial quantum yields, ranging between about 0.1 and 0.3 (Fig. 4) The wavelength where the intensity-normalized absorption and emission spectra cross provides a means for estimating $\mathscr{E}_{00}$ (Fig. 4c) [71–74]. For the **Aa** residues, $\mathscr{E}_{00}$ ranged from about 3 to 3.7 eV (Fig. 5c). The capability of the alkyloxy and the dialkylamine substituents to extend the π-conjugation of the aromatic rings leads to a decrease in $\mathscr{E}_{00}$ that is consistent with narrowing the HOMO-LUMO gaps of the residues. This effect, however, was pronounced only for strong electron-donating substituents placed at the *para* position to the N-terminal amides (5Pip and 5Hxm vs. 4Pip and 4Hxm, Fig. 5).

Similar comparison for the alkyloxy-derivatized residues reveals that the spectral features of Hox are red-shifted compared to these of Dmx (Fig. 5). This red spectral shifts for Hox vs. Dmx, are most likely due to the methoxy group at the 4th position of Dmx. An electron-donating group at the 4th position appears to cause blue spectral shifts. Even strong electron-donating groups, such as amines, placed at the 4th position, i.e. 4Hxm and 4Pip, result in **Aa** residues with spectral features similar to those of Met and Ant (Fig. 5).
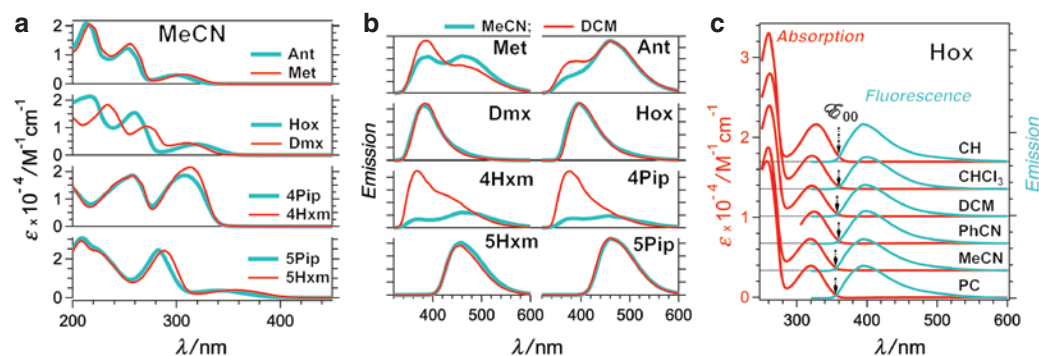
Fig. 4: UV/visible absorption and emission spectra of anthranilamide residues for various solvent media: propylene carbonate (PC), acetonitrile (MeCN), benzonitrile (PhCN), dichloromethane (DCM), chloroform (CHCl₃), and cyclohexane (CH). (a) Absorption spectra of the eight residues for MeCN. (b) Fluorescence spectra of the residues recorded for MeCN and DCM (λ_{ex} = 310 nm; each fluorescence spectrum was normalized by $\times(1 - 10^{-A(\lambda,ex)})^{-1}$). (c) Absorption and fluorescence spectra for Hox in the different solvents (λ_{ex} = 310 nm; each fluorescence spectrum was normalized to the height of the red-most band of the corresponding absorption spectrum; except for PC, the baselines of the spectra are elevated from 0 for improved visualization; the arrows point to wavelength, λ_{00}, of crossing point between the two spectra that is used for calculating the zero-to-zero energy, $\mathscr{E}_{00} = hc/\lambda_{00}$).
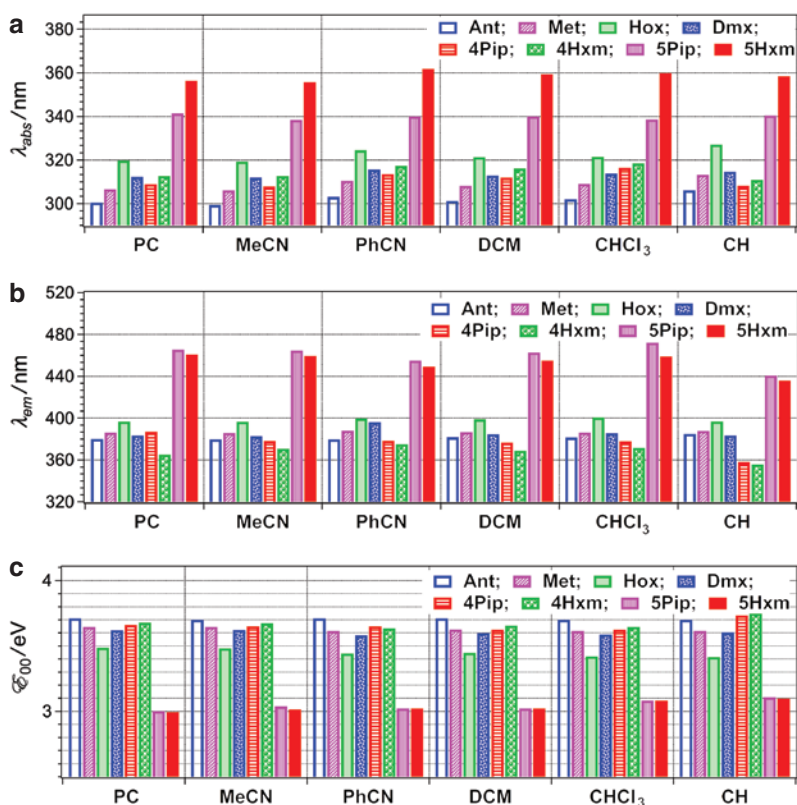
Fig. 5: Absorption and emission properties of the anthranilamide residues. (a) Wavelengths of the maxima of the most red-shifted bands of the absorption spectra of the eight residues for different solvents: propylene carbonate (PC), acetonitrile (MeCN), benzonitrile (PhCN), dichloromethane (DCM), chloroform (CHCl$_3$), and cyclohexane (CH). (b) Wavelengths of the maxima of the fluorescence spectra of the eight residues in different solvents (λ_{ex} = 310 nm). For each residue that, due to aggregation, exhibits two fluorescence bands, the wavelength of the blue-shifted maximum is reported. (c) Zero-to-zero energy values of the anthranilamide residues, extracted from wavelength where the normalized absorption and emission spectra cross (Fig. 4).

While $\mathscr{E}_{00}$ depends on the R$_1$ and R$_2$ substituents, the solvent polarity has insignificant to no effect on the spectral properties of the **Aa** residues (Figs. 4 and 5). This lack of substantial solvatochromism is consistent with our previous experimental observations and theoretical findings for Ant and 5Pip derivatives [45, 46]. The anthranilamides are, indeed, polar molecules. The observed lack of significant solvatochromism, therefore, suggests that photoexcitation of the **Aa** residues does not substantially alter their polarity. That is, the permanent ground-state dipoles have dominating effect on the ground- and excited-state polarity of the **Aa** conjugates.

Another feature revealed by the emission spectra of the **Aa** residues is their propensity to aggregate. As expected from our previous studies [46], two of the residues, Ant and Met, exhibit fluorescence bands with two peaks (Fig. 4b), the ratios between which are concentration dependent. We ascribe the red-shifted peak, the intensity of which increases with an increase in concentration, to aggregates that form at the excited and/or the ground state [46, 75–80]. The trends from this assignment of the fluorescence spectra indicate that the chlorinated hydrocarbons, such as DCM, tend to suppress aggregation (Fig. 4b).

In addition, 4Pip and 4Hxm also aggregate at μM concentrations when dissolved in some of the tested organic solvents (Fig. 4b). This finding was somewhat surprising because the residues with identical alkyl chains attached to them, 5Pip and 5Hxm, did not manifest detectable aggregation even at concentrations reaching 1 mM. These findings show that the position of substituents with alkyl chains (i.e. R$_1$ vs. R$_2$) pronouncedly affects the aggregation propensity of the **Aa** derivatives. To confirm this trend, other two residues, Hox and Dmx, that also contain alkyl chains at the 5th, also show a single fluorescence peak, indicating that they do not manifest detectable aggregation in the tested organic solvents (Fig. 4b).

Comparison between 4Pip and 4Hxm reveals an important trend about the dependence of the aggregation propensity on the structure of the substituents. Both residues aggregate when dissolved in most organic solvents at μM concentrations. In chlorinated solvents, however, while 4Pip exists as a monomer, 4Hxm manifests some propensity for aggregation (Fig. 4b). Both residues contain secondary amines at the 4th positions of their aromatic rings. Both substituents contain more than five carbons in their alkyl chains (piperidinyl for 4Pip, and hexyl and methyl for 4Hxm, Fig. 2). In fact, 4Hxm has a longer chain than 4Pip. Contrarily to correlating improved solubility with increased length of alkyl substituents, however, 4Hxm has a larger propensity for aggregation than 4Pip. In the piperidinyl substituents more carbons are located closer to the aromatic ring than in hexylmethylamine. This increase in the volume of the solvation cavity immediately next to the aromatic moieties (that may drive aggregation) appears to have dominant effect on improving the residue solubility. This trend indicates that long linear chains, such as hexyls, do not improve the solubility in organic solvents to the extent that branched substituents, such as piperidinyl, do.

Permanent electric dipoles and distribution of the frontier orbitals

Ab initio computational studies provide further key information about the electronic properties of the **Aa** residues and the dependence of these properties on the media polarity. Ground-state DFT calculations at the B3LYP/6-311 + G(d,p) level [81–83] performed using Gaussian 09 [84] revealed that the HOMOs and LUMOs of all eight **Aa** residues are predominantly localized on their aromatic rings (Fig. 6). For the residues with no substituents or with relatively weak electron-donating R_1 and R_2 groups, i.e. for Ant, Met, Hox and Dmx, the HOMOs extend over the N-terminal amide bond, while the LUMOs tend to delocalize over both amides (Fig. 6). Placing a strong electron-donating group on the 5th position (i.e. R_2 = dialkylamine) amplifies these orbital-delocalization trends (see 5Pip on Fig. 6, and 5Hxm in the Supplementary Material). Conversely, placing the same strong electron-donating groups on the 4th position shifts the delocalization of the HOMOs to the C-terminal amides (see 4Pip Fig. 6, and 4Hxm in the Supplementary Material).

To account for the solvent effects on the electronic properties of the **Aa** residues, we introduced DCM and MeCN to the calculations using a polarizable continuum model [85–87]. Inclusion of the solvents had no visible effect on the distribution of frontier orbitals (Fig. 6). Most importantly, the optimized structures of the eight **Aa** residues remain practically identical when varying the solvent media (see Supplementary Material). While the anthranilamides are polar molecules, principally because of the amide dipoles, these computational findings suggest that the preferential **Aa** conformation, with *trans* amides, is not affected by changes in the solvent polarity.

The permanent electric dipoles are the most important feature of the **Aa** residues, making them promising building blocks for electrets. The predicted dipole moment of Ant is about 4.7 D (Table 1), which is consistent with the contributions of 1.9 D from each of the two amides and of 0.9 D from the polarization due to the hydrogen bonding (Fig. 1) [48]. Adding methyl to the 5th position, such as in Met, slightly enhances the dipole (Table 1), which is consistent with the 5-methyl-induced polarization of the aromatic ring co-directionally with the total dipole from the amide and hydrogen bonds. This enhancement effect on the **Aa** dipole is even more pronounced for Hox, 5Hxm and 5Pip, where R_2 electron-donating groups have mesomeric, rather than inductive, effects on the aromatic ring (Table 1). Conversely, when an electron-donating group is at the 4th position, such as in 4Hxm and 4Pip, the substituent-induced polarization of the aromatic ring has a diminishing effect on the total residue dipole (Table 1).

Solvent polarity further enhances the magnitude of the **Aa** dipoles (Table 1). Because the electronic and structural properties of the **Aa** residues have a negligible dependence on the media, this polarity-driven enhancement can be attributed to the effect of the **Aa** dipoles on the solvent itself. As we have shown for simple aliphatic amides, such dipole enhancement results from the Onsager fields inside the solvation cavities of the solutes [66, 88]. The **Aa** dipoles polarize the solvent media in the proximity to the solvation cavities. This polarization increases the displacements between the centers of the positive and negative charges of the solvated **Aa** molecules, increasing the magnitudes of their total dipole moments.

Fig. 6: HOMOs and LUMOs of Ant, Met, 4Pip and 5Pip for the gas phase (GP) and for acetonitrile (MeCN), obtained from DFT calculations. For the computational studies, the alkyl chains at the C- and N-termini were truncated to C_2H_5. The residues are displayed with their N-termini oriented to the left and the C-termini – to the right. (See the Supplementary Material for the HOMOs and LUMOs of all eight residues.)

Discussion

The solvent effect on the permanent molecular dipoles has important implications on the CT properties of the anthranilamides. Others and we have shown that an increase in solvent polarity diminishes the dipole effects on CT [32, 33, 45], which is attributed to the screening of the dipole-generated electric field by the surrounding polar media. Concurrently, the media polarity enhances the dipole-generated field inside a solvated molecule [66]. Conversely, for the reported solvent effects on dipole-mediated CT, the electron donor and acceptor are linked in a manner that places both or either of them outside the solvation cavity containing the groups generating the dipole fields. That is, the sources of the permanent dipoles are frequently polypeptide helices, and the redox moieties involved in the CT are located at certain distance from the helix backbones, linked to side

chains of residues composing the polypeptide. Thus, while the electron-tunneling pathways may transverse through cavities with solvent-induced enhancement of dipolar fields, the solvation of the acceptor and/or of the donor, outside these cavities, principally affects the CT kinetics.

As an alternative to protein-derived structures, anthranilamide molecular electrets have the structural and electronic features for exploration of solvation dependence of dipole-mediated CT. The aromatic moieties, providing sites for charge hopping, are directly linked via amides that are responsible for the permanent dipole moments. Hence, the intertwining of the charge-hopping sites and the dipolar groups generating the fields situates them within the same solvation cavity.

While the dipole-generated fields of such electrets can guide the CT processes, the ability to tune energetics along the CT pathways should not be undermined. The electron-donating substituents stabilize positive charges, h^+, injected in the aromatic residues, as evident from the negative shifts in the reduction potentials of **Aa** oxidation when R_1 and R_2 are changed from hydrogen to alkyloxyls and to amines (Table 1). The ability to adjust the **Aa** reduction potentials over a range of 1 V shows a key advantage of anthranilamide CT electrets illustrating their promising potential and utility.

Frequently, potential wells with depth in the order of a few hundred millielectronvolts are responsible for undesired charge-trapping and charge-recombination, decreasing performance efficiencies of materials and devices [89–93]. For **Aa** residues, only a single change in the position of an amine from R_2 to R_1 lowers their HOMO energy with about 0.3 eV, which exceeds the thermal energy, k_BT, by more than an order of magnitude. Overall, the magnitude of the substituent effects on the electronic properties of the **Aa** residues is comparable with the energetics that governs CT processes responsible for the performance of electronic materials and devices.

Considering such applications, three of the residues, Dmx, 5Hxm and 5Pip, appear to have the most desirable characteristics. First, they all exhibit reversible electrochemical oxidation making them excellent sites for h^+ hopping. Indeed, the potentials of Hox, Met and Ant are positive enough to cause oxidative cleavage of the amide bonds [70] that sustain the structural integrity of the macromolecules these residues may compose. Therefore, their use may be limited to introducing them as tunneling barriers on the CT pathways. Conversely, 4Hxm and 4Pip present a curious case. Their reduction potentials do not appear positive enough to induce amide oxidation. Can 4Hxm and 4Pip, then, mediate h^+ hopping without oxidative cleavage? The cyclic voltammetry results indicate that 4Hxm$^{\bullet+}$ and 4Pip$^{\bullet+}$ have lifetimes much shorter than hundreds of milliseconds, making the cathodic waves undetectable. If the life of these radical cations, however, is longer than a few nanoseconds, 4Pip and 4Hxm still can be viable sites for h^+ hopping that does not cause irreversible damage of the molecular structures.

Second, 5Hxm, 5Pip and Dmx do not aggregate at hundreds of μM concentrations. This feature is important not only for solution phase studies, but also for processing materials composed of these residues. In addition to these three residues, the lack of aggregation propensities of Hox can also prove beneficial for macromolecular designs. While electronically Hox residues may be used solely for adding tunneling barriers along CT pathways, introducing Hox to anthranilamide macromolecules will improve their solubility in organic media. Again, 4Hxm and 4Pip appear to have an outlier-like behavior. The six-carbon alkyl chains of their R_1 substituents do not eliminated their propensity for aggregation. Polarizable chlorinated solvents appear to at least partially suppress the aggregation of the 4-amino residues. 4Hxm and 4Pip, however, tend to aggregate when dissolved in other organic solvents.

Overall, 5Hxm, 5Pip, Dmx and Hox appear as most viable building blocks for molecular electrets that can readily mediate efficient long-range CT. Indeed, this analysis is based on conjugates composed of single **Aa** residues. Although the electronic properties of anthranilamide oligomers have negligible dependence on the number of residues [46], the single-residue findings should be viewed as important guidelines, rather than strict rules. Therefore, we cannot rule out the potential utility of 4Hxm and 4Pip. The irreversible electrochemical oxidation and the aggregation propensity of 4Hxm and 4Pip are not truly desirable features. Before these two residues are tested as building blocks of **Aa** oligomers, it will be premature to decide how adverse these features may prove. Conversely, the energy levels of their HOMOs of the 4-amino **Aa** residues are located between of the HOMOs of Dmx and 5Pip, making 4Hxm and 4Pip still attractive candidates for the exploration of the diversity of the CT molecular electrets.

In living organisms, each of the 20 native amino acids has quite a difference relative abundance in the known proteins they compose [94]. Similarly, in the design of CT molecular electrets, not all the **Aa** residues need to be equally present. Some residues, such as 5Hxm and Hox, may play principal role in determining the structural and electronic characteristics of the molecular electrets. Other residues, such as Ant and Met, may be used scarcely as "dopants."

Conclusions

Their permanent dipole moments make anthranilamides attractive candidates for charge-transfer systems. Combinations of three types of electron-donating substituents at two possible positions yield a set of non-native **Aa** residues with diverse electronic properties. In proteomics, permutations using 20 native amino acids lead to countless structure–function relationships. We believe that, in a similar manner, the herein described non-native **Aa** residues are key building blocks for countless macromolecular systems with a wide range of unexplored electronic features.

References

[1] D. N. Beratan, C. Liu, A. Migliore, N. F. Polizzi, S. S. Skourtis, P. Zhang, Y. Zhang. *Acc. Chem. Res.* **48**, 474 (2015).

[2] U. Brandt. *BIOspektrum* **20**, 267 (2014).

[3] F. Sun, Q. Zhou, X. Pang, Y. Xu, Z. Rao. *Curr. Op. Struct. Biol.* **23**, 526 (2013).

[4] P. Venditti, L. Di Stefano, S. Di Meo. *Mitochondrion* **13**, 71 (2013).

[5] J. J. Warren, J. R. Winkler, H. B. Gray. *Coordinat. Chem. Rev.* **257**, 165 (2013).

[6] J. Barber, P. D. Tran. *J. Royal Soc. Interface* **10**, 20120984 (2013).

[7] G. Centi, S. Perathoner. Photoelectrochemical CO_2 activation toward artificial leaves in *Chem. Energ. Stor*, R. Schlögl (Ed.), pp. 379–400, Walter de Gruyter GmbH, Berlin/Boston (2013). ISBN 978-3-11-026407-4; e-ISBN 978-3-11-026632-0; http://www.degruyter.com/viewbooktoc/product/179232.

[8] K. S. Joya, Y. F. Joya, K. Ocakoglu, R. van de Krol. *Angew. Chem. Int. Edit.* **52**, 10426 (2013).

[9] D. G. Nocera. *Acc. Chem. Res.* **45**, 767 (2012).

[10] J. Michl. *Nat. Chem.* **3**, 268 (2011).

[11] S. Kirner, M. Sekita, D. M. Guldi. *Adv. Mater.* **26**, 1482 (2014).

[12] D. Gust, T. A. Moore, A. L. Moore. *Acc. Chem. Res.* **42**, 1890 (2009).

[13] D. L. DuBois. *Inorg. Chem.* **53**, 3935 (2014).

[14] C. Zhang, Y. Yan, Y. S. Zhao, J. Yao. *Acc. Chem. Res.* **47**, 3448 (2014).

[15] T. W. Ng, M. F. Lo, M. K. Fung, W. J. Zhang, C. S. Lee. *Adv. Mater.* **26**, 5569 (2014).

[16] T. Shears. *Phil. Trans. Royal Soc. A* **370**, 805 (2012).

[17] N. Nagaosa, Y. Tokura. *Physica. Scripta. T* **T146**, 014020 (2012).

[18] B. M. Savoie, N. E. Jackson, L. X. Chen, T. J. Marks, M. A. Ratner. *Acc. Chem. Res.* **47**, 3385 (2014).

[19] J. N. Israelachvili, K. Kristiansen, M. A. Gebbie, D. W. Lee, S. H. Donaldson, S. Das, M. V. Rapp, X. Banquy, M. Valtiner, J. Yu. *J. Phys. Chem. B* **117**, 16369 (2013).

[20] M. W. Williams. *AIP Advances* **2**, 010701 (2012).

[21] S. Upadhyayula, T. Quinata, S. Bishop, S. Gupta, N. R. Johnson, B. Bahmani, K. Bozhilov, J. Stubbs, P. Jreij, P. Nallagatla, V. I. Vullev. *Langmuir* **28**, 5059 (2012).

[22] K. Chau, B. Millare, A. Lin, S. Upadhyayula, V. Nuñez, H. Xu, V. I. Vullev. *Microfluid. Nanofluid.* **10**, 907 (2011).

[23] B. Millare, M. Thomas, A. Ferreira, H. Xu, M. Holesinger, V. I. Vullev. *Langmuir* **24**, 13218 (2008).

[24] V. Nuñez, S. Upadhyayula, B. Millare, J. M. Larsen, A. Hadian, S. Shin, P. Vandrangi, S. Gupta, H. Xu, A. P. Lin, G. Y. Georgiev, V. I. Vullev. *Anal. Chem.* **85**, 4567 (2013).

[25] C. Hong, D. Bao, M. S. Thomas, J. M. Clift, V. I. Vullev. *Langmuir* **24**, 8439 (2008).

[26] V. I. Vullev, J. Wan, V. Heinrich, P. Landsman, P. E. Bower, B. Xia, B. Millare, G. Jones, II. *J. Am. Chem. Soc.* **128**, 16062 (2006).

[27] G. Jones, II, V. I. Vullev. *J. Phys. Chem. A* **106**, 8213 (2002).

[28] G. Jones, II, V. I. Vullev. *Photochem. Photobiol. Sci.* **1**, 925 (2002).

[29] D. A. Doyle, J. M. Cabral, R. A. Pfuetzner, A. L. Kuo, J. M. Gulbis, S. L. Cohen, B. T. Chait, R. MacKinnon. *Science* **280**, 69 (1998).

[30] R. Dutzler, E. B. Campbell, M. Cadene, B. T. Chait, R. MacKinnon. *Nature* **415**, 287 (2002).

[31] S. Tanaka, R. A. Marcus. *J. Phys. Chem. B* **101**, 5031 (1997).

[32] E. Galoppini, M. A. Fox. *J. Am. Chem. Soc.* **118**, 2299 (1996).

[33] M. A. Fox, E. Galoppini. *J. Am. Chem. Soc.* **119**, 5277 (1997).

[34] S. Yasutomi, T. Morita, Y. Imanishi, S. Kimura. *Science* **304**, 1944 (2004).

[35] Y.-G. K. Shin, M. D. Newton, S. S. Isied. *J. Am. Chem. Soc.* **125**, 3722 (2003).

[36] B. Giese, M. Graber, M. Cordes. *Curr. Op. Chem. Biol.* **12**, 755 (2008).

[37] H. B. Gray, J. R. Winkler. *Q. Rev. Biophy.* **36**, 341 (2003).

[38] H. B. Gray, J. R. Winkler. *Proc. Natnl. Acad. Sci. USA* **102**, 3534 (2005).

[39] V. I. Vullev, G. Jones, II. *Res. Chem. Intermed.* **28**, 795 (2002).

[40] G. Jones, II, V. I. Vullev. *Org. Lett.* **4**, 4001 (2002).

[41] G. Jones, II, V. Vullev, E. H. Braswell, D. Zhu. *J. Am. Chem. Soc.* **122**, 388 (2000).

[42] G. Jones, II, L. N. Lu, V. Vullev, D. Gosztola, S. Greenfield, M. Wasielewski. *Bioorg. Med. Chem. Lett.* **5**, 2385 (1995).

[43] G. Jones, II, X. Zhou, V. I. Vullev. *Photochem. Photobiol. Sci.* **2**, 1080 (2003).

[44] S. L. Mayo, W. R. Ellis Jr., R. J. Crutchley, H. B. Gray. *Science* **233**, 948 (1986).

[45] D. Bao, S. Upadhyayula, J. M. Larsen, B. Xia, B. Georgieva, V. Nunez, E. M. Espinoza, J. D. Hartman, M. Wurch, A. Chang, C.-K. Lin, J. Larkin, K. Vasquez, G. J. O. Beran, V. I. Vullev. *J. Am. Chem. Soc.* **136**, 12966 (2014).

[46] B. Xia, D. Bao, S. Upadhyayula, G. Jones, V. I. Vullev. *J. Org. Chem.* **78**, 1994 (2013).

[47] V. I. Vullev. *J. Phys. Chem. Lett.* **2**, 503 (2011).

[48] M. K. Ashraf, R. R. Pandey, R. K. Lake, B. Millare, A. A. Gerasimenko, D. Bao, V. I. Vullev. *Biotechnol. Progr.* **25**, 915 (2009).

[49] I. Huc. *Eur. J. Org. Chem.* **2004**, 17 (2004).

[50] L. Sebaoun, V. Maurizot, T. Granier, B. Kauffmann, I. Huc. *J. Am. Chem. Soc.* **136**, 2168 (2014).

[51] R. Orlowski, O. Vakuliuk, M. P. Gullo, O. Danylyuk, B. Ventura, B. Koszarna, A. Tarnowska, N. Jaworska, A. Barbieri, D. T. Gryko. *Chem. Commun.* **51**, 8284 (2015).

[52] N. Chandramouli, Y. Ferrand, G. Lautrette, B. Kauffmann, C. D. Mackereth, M. Laguerre, D. Dubreuil, I. Huc. *Nat. Chem.* **7**, 334 (2015).

[53] Q. A. Gan, Y. Ferrand, C. Y. Bao, B. Kauffmann, A. Grelard, H. Jiang, I. Huc. *Science* **331**, 1172 (2011).

[54] A. S. Voisin-Chiret, S. Rault. *Pure Appl. Chem.* **84**, 2467 (2012).

[55] D. W. Zhang, X. Zhao, Z. T. Li. *Acc. Chem. Res.* **47**, 1961 (2014).

[56] P. Prabhakaran, G. Priya, G. J. Sanjayan. *Angew. Chem. Int. Edit.* **51**, 4006 (2012).

[57] M. Wolffs, N. Delsuc, D. Veldman, N. Van Anh, R. M. Williams, S. C. J. Meskers, R. A. J. Janssen, I. Huc, A. P. H. J. Schenning. *J. Am. Chem. Soc.* **131**, 4819 (2009).

[58] Y. Hamuro, S. J. Geib, A. D. Hamilton. *J. Am. Chem. Soc.* **118**, 7529 (1996).

[59] G. Mansour, W. Creedon, P. C. Dorrestein, J. Maxka, J. C. MacDonald, R. Helburn. *J. Org. Chem.* **66**, 4050 (2001).

[60] C. O. Kappe, B. Pieber, D. Dallinger. *Angew. Chem. Int. Edit.* **52**, 1088 (2013).

[61] A. de la Hoz, A. Diaz-Ortiz, A. Moreno. *Chem. Soc. Rev.* **34**, 164 (2005).

[62] D. Rehm, A. Weller. *Israel. J. Chem.* **8**, 259 (1970).

[63] S. Trasatti. *Pure Appl. Chem.* **58**, 955 (1986).

[64] D. Bao, S. Ramu, A. Contreras, S. Upadhyayula, J. M. Vasquez, G. Beran, V. I. Vullev. *J. Phys. Chem. B* **114**, 14467 (2010).

[65] D. Bao, B. Millare, W. Xia, B. G. Steyer, A. A. Gerasimenko, A. Ferreira, A. Contreras, V. I. Vullev. *J. Phys. Chem. A* **113**, 1259 (2009).

[66] S. Upadhyayula, D. Bao, B. Millare, S. S. Sylvia, K. M. M. Habib, K. Ashraf, A. Ferreira, S. Bishop, R. Bonderer, S. Baqai, X. Jing, M. Penchev, M. Ozkan, C. S. Ozkan, R. K. Lake, V. I. Vullev. *J. Phys. Chem. B* **115**, 9473 (2011).

[67] J. Hu, B. Xia, D. Bao, A. Ferreira, J. Wan, G. Jones, V. I. Vullev. *J. Phys. Chem. A* **113**, 3096 (2009).

[68] J. Wan, A. Ferreira, W. Xia, C. H. Chow, K. Takechi, P. V. Kamat, G. Jones, V. I. Vullev. *J. Photochem. Photobiol. A* **197**, 364 (2008).

[69] M. Born. *Z. Phys.* **1**, 45 (1920).

[70] J. F. Odonnell, C. K. Mann. *J. Electroanal. Chem.* **13**, 157 (1967).

[71] S. Guo, D. Bao, S. Upadhyayula, W. Wang, A. B. Guvenc, J. R. Kyle, H. Hosseinibay, K. N. Bozhilov, V. I. Vullev, C. S. Ozkan, M. Ozkan. *Adv. Funct. Mater.* **23**, 5199 (2013).

[72] V. I. Vullev, G. Jones. *Tetrahedr. Lett.* **43**, 8611 (2002).

[73] G. Jones, II, D. Yan, J. Hu, J. Wan, B. Xia, V. I. Vullev. *J. Phys. Chem. B* **111**, 6921 (2007).

[74] H. Lu, D. Bao, M. Penchev, M. Ghazinejad, V. I. Vullev, C. S. Ozkan, M. Ozkan. *Adv. Sci. Lett.* **3**, 101 (2010).

[75] G. Jones, II, V. I. Vullev. *J. Phys. Chem. A* **105**, 6402 (2001).
[76] G. Jones, II, V. I. Vullev. *Org. Lett.* **3**, 2457 (2001).
[77] J. M. Vasquez, A. Vu, J. S. Schultz, V. I. Vullev. *Biotechnol. Progr.* **25**, 906 (2009).
[78] W. Wang, S. Guo, M. Penchev, J. Zhong, J. Lin, D. Bao, V. Vullev, M. Ozkan, C. S. Ozkan. *J. Nanosci. Nanotechnol.* **12**, 6913 (2012).
[79] M. Ghazinejad, J. R. Kyle, S. Guo, D. Pleskot, D. Bao, V. I. Vullev, M. Ozkan, C. S. Ozkan. *Adv. Funct. Mater.* **22**, 4519 (2012).
[80] V. I. Vullev, H. Jiang, G. Jones, II. *Topics Fluoresc. Spectrosc.* **10**, 211 (2005).
[81] A. D. Becke. *J. Chem. Phys.* **98**, 5648 (1993).
[82] C. T. Lee, W. T. Yang, R. G. Parr. *Phys. Rev. B* **37**, 785 (1988).
[83] R. Krishnan, J. S. Binkley, R. Seeger, J. A. Pople. *J. Chem. Phys.* **72**, 650 (1980).
[84] M. J. Frisch et al., Gaussian 09, Revision A.1, Gaussian Inc. Wallingford CT, 2009.
[85] E. Cances, B. Mennucci. *J. Math. Chem.* **23**, 309 (1998).
[86] B. Mennucci, E. Cances, J. Tomasi. *J. Phys. Chem. B* **101**, 10506 (1997).
[87] E. Cances, B. Mennucci, J. Tomasi. *J. Chem. Phys.* **107**, 3032 (1997).
[88] L. Onsager. *J. Am. Chem. Soc.* **58**, 1486 (1936).
[89] X. Y. Zhu, Q. Yang, M. Muntwiler. *Acc. Chem. Res.* **42**, 1779 (2009).
[90] R. D. Pensack, J. B. Asbury. *J. Phys. Chem. Lett.* **1**, 2255 (2010).
[91] J. Guo, H. Ohkita, H. Benten, S. Ito. *J. Am. Chem. Soc.* **132**, 6154 (2010).
[92] M. Muntwiler, Q. Yang, W. A. Tisdale, X. Y. Zhu. *Phys. Rev. Lett.* **101**, 196403 (2008).
[93] H. Scher, S. Rackovsky. *J. Chem. Phys.* **81**, 1994 (1984).
[94] A. Moura, M. A. Savageau, R. Alves. *PLoS One* **8**, e77319 (2013).